

Angiostatin Overexpression in Morris Hepatoma Results in Decreased Tumor Growth but Increased Perfusion and Vascularization

Kerstin Schmidt, MS¹⁻³; Johannes Hoffend MD³; Annette Altmann, PhD^{2,3}; Ludwig G. Strauss, MD, PhD²; Antonia Dimitrakopoulou-Strauss, MD²; Britta Engelhardt, MD¹; Dirk Koczan, MD⁴; Jörg Peter, PhD⁵; Thomas J. Dengler, MD⁶; Walter Mier, PhD²; Michael Eisenhut, PhD⁷; Uwe Haberkorn, MD, PhD^{2,3}; and Ralf Kinscherf, PhD¹

¹Department of Anatomy and Cell Biology III, University of Heidelberg, INF 307, Heidelberg, Germany; ²Clinical Cooperation Unit Nuclear Medicine, DKFZ and University of Heidelberg, INF 280, Heidelberg, Germany; ³Department of Nuclear Medicine, University of Heidelberg, INF 400, Heidelberg, Germany; ⁴Department of Immunology, University of Rostock, Rostock, Germany; ⁵Department of Biophysics and Medical Radiation Physics, DKFZ, INF 280, Heidelberg, Germany; ⁶Department of Internal Medicine III, INF 410, University of Heidelberg, Germany; and ⁷Department of Radiopharmaceutical Chemistry, German Cancer Research Centre, Heidelberg, Germany

Growth of malignant tumors is dependent on sufficient blood supply. Thus, inhibition of tumor angiogenesis is emerging as a promising target in the treatment of malignancies. Human angiostatin (hANG) is one of the most potent inhibitors of endothelial cell proliferation, angiogenesis, and tumor growth in vivo. However, its mechanisms operating in vivo are not well understood. **Methods:** To obtain more information about functional changes in the angiogenic process, we established Morris hepatoma (MH3924A) cell lines expressing hANG (hANG-MH3924A). The effects of hANG expression on proliferation and apoptosis of human umbilical vein endothelial cells (HUVECs) were measured in coculture experiments in vitro. To evaluate changes in tumor perfusion and blood volume, H₂¹⁵O and ⁶⁸Ga-DOTA-albumin (DOTA is 1,4,7,10-tetraazacyclododecane-*N,N,N',N'*-tetraacetic acid) were used for PET studies in vivo. Additionally, immunohistologic quantification of vascularization, apoptosis, and proliferation as well as gene array analyses were performed. **Results:** Our in vitro experiments demonstrate reduced proliferation and increased apoptosis in HUVECs when being cocultured with hANG-MH3924A. In support, tumor growth of hANG-MH3924A is diminished by 95% in vivo. However, tumor perfusion and blood volume are increased in hANG-MH3924A corresponding to an increased microvessel density. Furthermore, hANG-transfected tumors show changes in expression of genes related to apoptosis, stress, signal transduction, and metabolism. **Conclusion:** hANG expression leads to inhibition of tumor growth, increased apoptosis, and changes in the expression of multiple genes involved in stress reactions, signal transduction, and apoptosis, which indicates a multifactorial reaction of tumors. An enhanced microvessel density is seen as part of these reactions and is associated with increased perfusion as measured by PET.

Key Words: angiogenesis; gene therapy; PET; angiostatin; perfusion

J Nucl Med 2006; 47:543–551

Tumor growth is angiogenesis dependent (1). Thus, inhibition of tumor angiogenesis is emerging as a promising target in the treatment of malignancies as well as for the prevention of cancer recurrence or metastasis (2). Novel strategies, including endogenous antiangiogenic agents, which starve tumors by disturbing blood supply, have been shown to be effective in preclinical models. The advantages of focusing on blood supply are prevention of drug resistance and a highly targeted therapy of a variety of tumor entities (3). Human angiostatin (hANG), a cleavage product of plasminogen, is one of the most potent antiangiogenic agents currently known (4). ANG exhibits profound inhibition of endothelial cell proliferation and migration in vitro and angiogenesis in vivo (5). Systemic administration of recombinant ANG inhibited angiogenesis and increased the apoptotic rate in several tumor models followed by tumor regression (6). The formation of ANG implicates metalloproteinases or serine proteinases produced by tumor cells (7) or by tumor-infiltrating macrophages (8). However, the molecular mechanisms of ANG treatment in vivo remain ill defined. Therefore, monitoring of antiangiogenic approaches with functional imaging and histomorphometric analyses are desirable to deliver information about physiologic effects caused by these therapeutic modalities. To provide a noninvasive, functional relevant measure of angiogenesis and to obtain functional data in animals and humans, MRI, CT, ultrasonography, optical imaging, and PET have been proposed (9). Especially PET using H₂¹⁵O

Received Aug. 26, 2005; revision accepted Nov. 21, 2005.

For correspondence or reprints contact: Uwe Haberkorn, MD, PhD, Department of Nuclear Medicine, University of Heidelberg, INF 400, Heidelberg, 69120, Germany.

E-mail: uwe_haberkorn@med.uni-heidelberg.de

provides a quantitative measure of tissue perfusion—that is, blood flow and blood volume in tumors (9). Furthermore, recent data present evidence that ^{68}Ga -DOTA-albumin (DOTA is 1,4,7,10-tetraazacyclododecane-*N,N',N'',N'''*-tetraacetic acid) PET can be used as a blood-pool marker in vivo (10). The aim of this study was to evaluate the effects of hANG gene transfer on tumor growth and changes in perfusion or blood volume relating in vivo measurements with PET to immunohistochemistry and gene expression analysis.

MATERIALS AND METHODS

Cell Culture and Generation of Recombinant Cells

Cells were cultured (37°C, 95% air/5% CO_2) in RPMI 1640 medium (Gibco BRL) supplemented with 292 mg/L glutamine and 20% fetal calf serum (FCS).

hANG Gene Transfer: Northern and Western Blots

MH3924A cells were transfected with hANG (pGT60hAngio-statin; InvivoGen) expression vectors. The hANG protein consists of 385 amino acids, including the first 4 kringle structures. Stable cell lines were generated after lipofection of MH3924A cells by hygromycin selection (425 $\mu\text{g}/\text{mL}$) for 4 wk. RNA was isolated using TRIZOL reagent (Roche) and messenger RNA (mRNA) expression was assessed by Northern blots using radioactively labeled probes delivered by digestion from corresponding plasmids. Secretion of hANG protein from selected clones into cell culture media was verified by Western blots. Conditioned medium was produced by culture of 10^6 transfected Morris hepatoma cells in OptiMem medium (Invitrogen) for 48 h. hANG protein was isolated from medium by incubation with L-lysine-Sepharose matrix followed by 3 washing steps and elution with sodium dodecyl sulfate–polyacrylamide gel electrophoresis sample buffer. After gel electrophoresis, protein was immunoblotted on a polyvinylidene fluoride membrane using polyclonal rabbit anti-hANG (2 $\mu\text{g}/\text{mL}$; Oncogene) antibodies and the ECL Western Blotting detection reagent (Amersham Biosciences).

Measurement of Apoptotic or Proliferating Cells

Human umbilical vein endothelial cells (HUVECs) were isolated as described (11) and cultured in supplemented (4 ng/mL basic fibroblast growth factor, 20% FCS, 292 mg/L glutamine, 100,000 IU/L penicillin, 100 mg/L streptomycin) M199 medium. After 3 d of coculture with wild-type (WT)- or hANG-MH3924A in a “without contact” system (pore size, 3 μm ; BD Biosciences), proliferation of HUVECs was determined by methyl- ^3H -thymidine (^3H -TdR) (Amersham-Buchler) incorporation following treatment with 0.5 mol/L perchloric acid/1 mol/L NaOH and apoptosis was measured in unfixed cells by YO-PRO-1 (Invitrogen) staining as described earlier (12). Coculture experiments were done in triplicate in 2 independent experiments.

Animal Studies

ACI and RNU (nude) rats were supplied by Charles River Laboratories. All animal studies were performed in compliance with the national laws relating to the conduct of animal experimentation. The in vitro doubling time of the cell lines used was 16.95 h for WT- and 17.4 h for hANG-MH3924A cells. After inoculation of WT or hANG cell suspensions (2×10^6 cells per animal) subcutaneously into the thigh of ACI or RNU rats, tumor growth was measured using calipers. Perfusion and blood volume

in tumors with diameters between 10 and 13 mm (8–19 d after transplantation for WT-MH3924A and 37 and 57 d for hANG-MH3924A) were examined after intravenous bolus injection of 70–150 MBq H_2^{15}O in 0.3 mL and 5–10 MBq ^{68}Ga -labeled albumin [^{68}Ga -DOTA-albumin] (same animals and session; the albumin PET scan was performed after the activity of H_2^{15}O decayed). All PET studies were done as dynamic measurements (20×3 s, 6×10 s, 4×15 s, and 6×30 s for H_2^{15}O and 12×10 s, 3×20 s, 4×30 s, and 10×60 s for ^{68}Ga -DOTA-albumin) acquired in 2-dimensional (2D) mode using a matrix of 256×256 on an ECAT HR+ (Siemens/CTI) scanner (pixel size, $2.277 \times 2.777 \times 2.425$ mm; transaxial resolution, 4.3 mm). A transmission scan was done for 10 min before tracer administration with 3 rotating germanium pin sources to obtain cross sections for attenuation correction. After iterative reconstruction (ordered-subsets expectation maximization; 8 subsets, 16 iterations), dynamic PET data were evaluated following definition of volumes of interest (VOIs) as described earlier using the PMOD software package (13). Time-activity curves were created using VOIs, which consist of several regions of interest (ROIs) over the target area. Irregular ROIs were drawn manually. Perfusion studies using H_2^{15}O were evaluated using a 1-tissue-compartment model (13). For the input function, we used the mean value of the VOI data obtained from the heart. ROIs were defined at 3–6 s after bolus injection in at least 3 consecutive slices (2.4-mm thickness) surrounded by 2 slices showing the heart in each direction. This approach was based on the findings of Ohtake et al. showing that the input function can be retrieved from the image data with acceptable accuracy (14). The heart weight and heart volume of a 250-g rat are 1.0 g and 1.2 mL, respectively (15). This results in an estimated recovery error of 10%, which can be neglected for the purposes of this study. The ^{68}Ga -DOTA-albumin uptake was expressed as the mean standardized uptake value (SUV) between 10 and 15 min after injection when the time-activity curve reaches a plateau. The SUV is defined as: tissue concentration [Bq/g]/(injected dose [Bq]/body weight [g]) (10).

Tissue Preparation and Immunohistochemistry

Rat tumors were fixed with immunohistochemistry zinc fixative (BD Biosciences), 4% paraformaldehyde (and embedded in paraffin), or shock-frozen in liquid nitrogen-cooled isopentane and kept in a freezer at -70°C . Immunohistochemistry of the tumors was performed on 6- μm cryostat sections according to procedures as described (12,16). For immunohistochemical investigations, monoclonal antibody mouse antirat-CD31 (1:500; BD Biosciences), mouse anti- α -actin (1:100; Roche), mouse antiproliferating cell nuclear antigen (PCNA; 1:500; DakoCytomation), or mouse antirat CD11b (1:500; BD Biosciences) was applied. Negative controls were performed using control immunoglobulin or omission of the primary antibody.

Apoptosis was measured on paraffin-embedded tumor cross sections by the terminal deoxynucleotidyl transferase (TdT)-mediated dUTP nick end labeling (TUNEL) technique using a commercial kit (Oncor).

Morphometric Analysis

Immunoreactive cells were recorded by video camera (Olympus HCC-3600 P high gain) and quantified using a computer-assisted image analysis system (VIBAM 0.0-VFG 1-frame grabber) as described earlier (16). Morphometric analyses were performed

twice by 2 independent observers (interobserver variability, <5%).

Gene Arrays

Aliquots of WT- and hANG-MH3924A tumors obtained from the periphery were stored in TRIzol to extract RNA according to the manufacturer's specifications. RNA was purified using the RNeasy kit (Qiagen Inc.) and quality was photometrically tested by the 280:260 ratio and on agarose gel. Gene chip expression arrays were performed using "The Rat Genome U34 Set" (Affimetrix Inc.). The RNAs of hANG- ($n = 5$) and WT-MH3924A ($n = 7$) tumors were pooled and evaluated on separate gene chips as described earlier (16). The complete experiment was repeated twice, revealing a high correlation of signals in both experiments (hANG: $r = 0.96$ [tumor], $r = 0.98$ [cells]).

Statistical Methods

Results are presented as mean \pm SEM. Statistical analyses were performed by the Mann-Whitney U test or by the unpaired Student t test using the SIGMASTAT program (Jandel Scientific). $P \leq 0.05$ was considered statistically significant.

RESULTS

Inhibition of Proliferation and Induction of Apoptosis in Coculture Experiments with HUVECs

Successful transfer of the hANG gene into MH3924A (hANG-MH3924A) and overexpression of the hANG gene were determined by Northern and Western blotting (Figs. 1A and 1B). A protein with a molecular weight of 56 kDa was identified in cell culture medium of hANG-overexpressing cells (Fig. 1B).

After treatment with perchloric acid/NaOH yielding an acid-insoluble (representing nucleic acids and proteins) and an acid-soluble (representing unbound radioactivity in acid-soluble molecules that are not in DNA and proteins—e.g.,

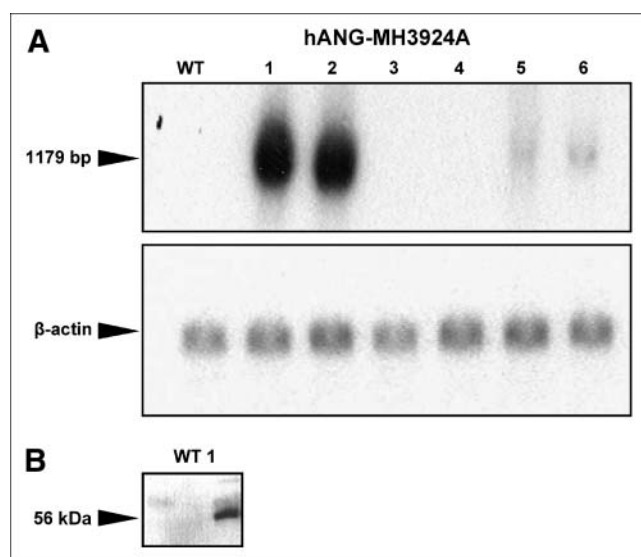


FIGURE 1. Expression of hANG in clones of MH3924A. (A) Northern blot. (B) Western blot. Representative blots are shown. α -Tubulin or β -actin was used as internal control. bp = base pairs.

cytoplasm, small molecules) fraction, the proliferation of HUVECs was measured by ^3H -TdR incorporation into DNA. HUVECs cocultured with WT-MH3924A showed a 30% increase of proliferation in comparison to HUVECs cultured alone. The proliferation rate of HUVECs decreased significantly by 65% when cocultured with h-ANG-MH3924A in comparison with coculture with WT-MH3924A cells (Fig. 2A).

Furthermore, the percentage of apoptotic HUVECs cocultured with hANG-MH3924A increased 3.5-fold ($P < 0.05$) compared with coculture with WT-MH3924A (Fig. 2B).

Inhibition of Tumor Growth and Proliferation and Induction of Apoptosis in hANG-Overexpressing MH3924A Tumors In Vivo

After inoculation of tumor cell suspensions, we examined growth of WT- and hANG-MH3924A tumors in rats, including histologic analysis of proliferation, necrosis, apoptosis, and the content of oxidative stress inducing cells in these tumors.

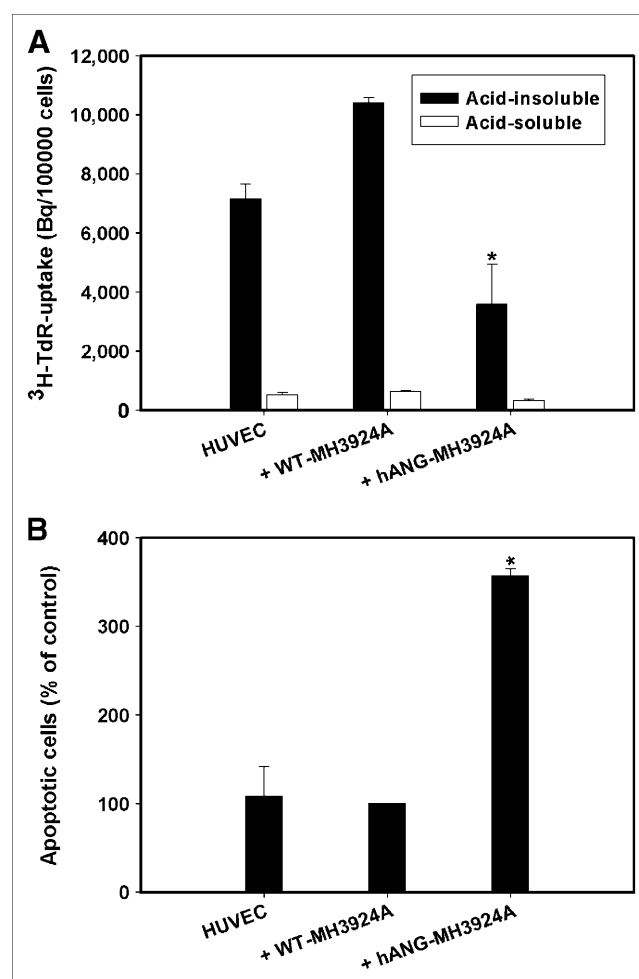


FIGURE 2. Proliferation and apoptosis of HUVECs cocultured with WT-MH3924A or hANG-MH3924A. (A) Proliferation (acid-soluble and acid-insoluble fractions of thymidine uptake). (B) Apoptosis. Values are shown as mean \pm SEM (* $P < 0.05$ vs. WT-MH3924A).

At 36 d after inoculation in ACI rats, *in vivo* growth of hANG-MH3924A tumors was reduced by 95% (Fig. 3). In *in vivo* experiments, using a mixture of overexpressing cells (10% or 90%, respectively) and WT-MH3924, revealed that 36 d after inoculation tumor growth was inhibited by about 45% (90% hANG-MH3924A) and 20% (10% hANG-MH3924A) in comparison with the WT-MH3924A tumors. To exclude immunologic effects as possible causes for growth inhibition, we measured tumor size of hANG- and WT-MH3924A in athymic (nude) RNU rats. Eighteen days after inoculation, 90% suppression of tumor growth was noted in animals bearing hANG-overexpressing tumors (absolute value, $300 \pm 73 \mu\text{L}$; $n = 4$) in comparison with animals with WT-MH3924A (absolute value, $3,600 \pm 400 \mu\text{L}$; $n = 5$) (data not shown).

Immunohistochemistry demonstrated that the proliferation rate of hANG tumors (identified by PCNA staining) was significantly decreased (55%) (Fig. 4A). Additionally, the density of apoptotic cells increased (100%) in hANG-MH3924A tumors (Fig. 4B), whereas the density of p53 immunoreactive cells per millimeter² was comparable in both groups (data not shown). In hANG-MH3924A, the necrotic area decreased significantly ($P < 0.01$) to $5.3\% \pm 0.8\%$ in comparison with WT-MH3924A ($21.9\% \pm 4.2\%$). Furthermore, in hANG-MH3924A tumors, the percentage of CD11b immunoreactive cells ($8.4\% \pm 0.9\%$) decreased significantly ($P < 0.001$) in comparison with WT-MH3924A ($29.6\% \pm 3.8\%$).

Increased Perfusion and Blood Volume in hANG-Overexpressing Hepatomas: PET and Immunohistomorphometry

Given that hANG has been described as a strong inhibitor of angiogenesis, we expected significant differences in tissue perfusion and blood volume in tumors overexpressing angiostatin. For tissue perfusion, dynamic PET measurements with H_2^{15}O were performed. Pharmacokinetic

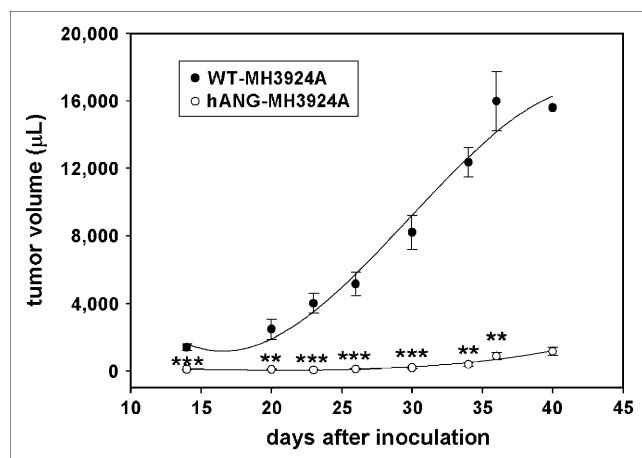


FIGURE 3. Tumor growth of WT-MH3924A and hANG-MH3924A tumors until 40 d after inoculation. Values are shown as mean \pm SEM (** $P < 0.001$; * $P < 0.01$; vs. WT-MH3924A).

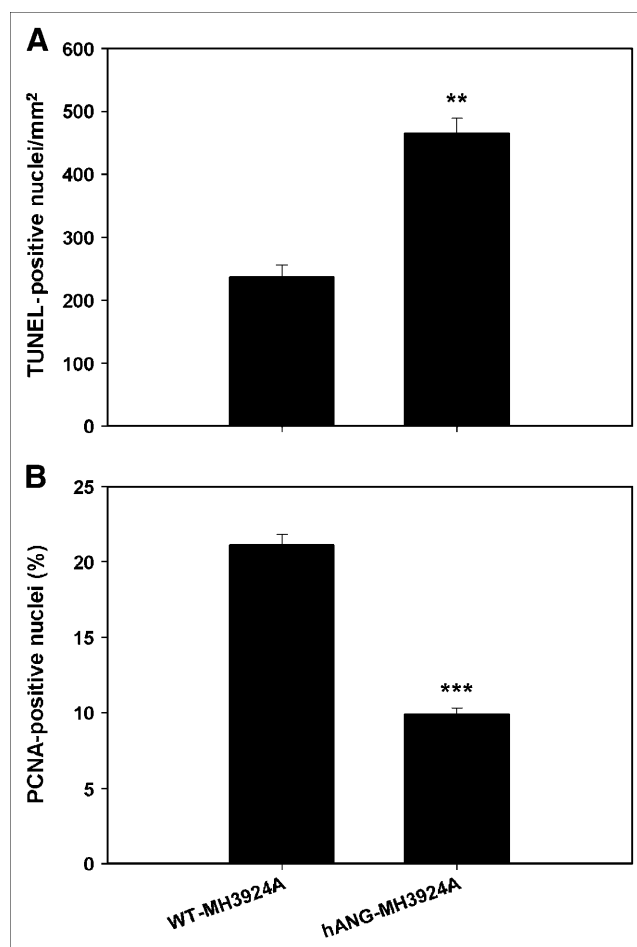


FIGURE 4. Histomorphometric analyses of apoptotic and proliferative cells (as indicated by TUNEL technique [A] or PCNA staining [B]) in WT-MH3924A and hANG-MH3924A tumors. Cell density (nuclei/mm²) or percentage of positive cells was quantified by analyzing 5 ROIs ($n = 6$ each group). Values are shown as mean \pm SEM (** $P < 0.001$; * $P < 0.01$ vs. WT-MH3924A).

analysis of the PET data showed that, on the average, tumor perfusion, represented as the transport rate K_1 (in $\text{mL} \times \text{mL tissue}^{-1} \times \text{min}^{-1}$), increased significantly ($P = 0.001$) in hANG-MH3924A (0.77 ± 0.04) in comparison with WT-MH3924A (0.43 ± 0.04 ; Fig. 5A). The k_2 value did not differ in hANG-MH3924A (0.82 ± 0.03) in comparison with WT-MH3924A (0.73 ± 0.10 ; Fig. 5B). The fractional volume of distribution (DV) increased significantly in hANG-MH3924A (0.95 ± 0.07 ; $P = 0.03$) compared with WT-MH3924A (0.65 ± 0.11 ; Fig. 5C), whereas the vascular fraction (VB) did not differ significantly between WT-MH3924A (0.02 ± 0.01) and hANG-MH3924A (0.05 ± 0.02) tumors (Fig. 5D).

To obtain noninvasive data about the perfused intravascular space of the tumor, dynamic blood-pool PET with ^{68}Ga -DOTA-albumin was conducted and mean SUVs were calculated. Our blood-pool PET studies demonstrated a significantly increased blood volume of 28% in hANG-MH3924A (0.68 ± 0.04) compared with WT-MH3924A

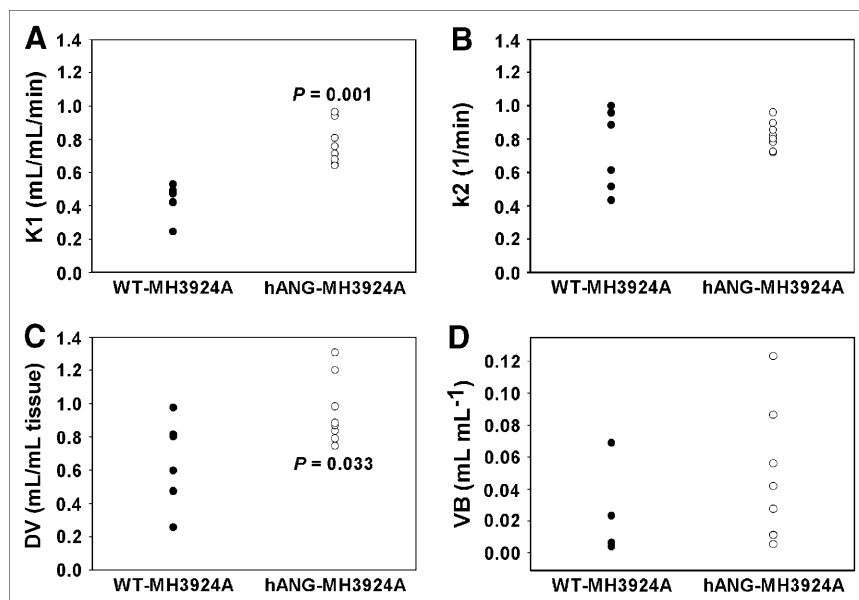


FIGURE 5. H₂¹⁵O PET. Tumor perfusion (K_1 , k_2 , DV, and VB values) measured in WT-MH3924A ($n = 7$) and hANG-MH3924A ($n = 8$) of ACI rats; 2D acquisition (1-tissue compartment model). hANG-expressing tumors showed a significantly increased K_1 (A), whereas k_2 remained unchanged (B). The fractional volume of distribution (DV) increased significantly in hANG-MH3924A (C), whereas the vascular fraction (VB) showed no difference (D).

(0.49 ± 0.07) (Fig. 6). To allow a comparison with the H₂¹⁵O study, tumor-to-heart ratios were calculated at 45–65 s after tracer administration with significantly ($P = 0.002$) increased values for hANG-MH3924A (0.8 ± 0.19) as compared with WT-MH3924A (0.47 ± 0.12) for H₂¹⁵O. The ratios for albumin showed similar changes (0.17 ± 0.05 for hANG-MH3924A and 0.09 ± 0.02 for WT-MH3924A with $P = 0.007$).

The most commonly used vascular marker, α -actin, is expressed by mural cells of most arterioles and venules, but not in capillaries (9). In ACI rats we found that the α -actin immunoreactive area is similar in hANG- and WT-MH3924A tumors in the periphery as well as in the center; however, it is twice as high in the periphery in comparison with the

center (Fig. 7A). Using the generally accepted method to determine microvessel density by measuring the CD31 immunoreactive area in angiogenic “hot spots” in the periphery (17), we found a 40% increase in hANG-MH3924A tumors (Fig. 7B). Microvessel density is 2–3 times higher in the periphery in comparison with the center. In addition, the mean number of blood vessels was significantly increased in hANG- (330.14 ± 28.80 per mm²) in comparison with WT-MH3924A tumors (222.02 ± 25.58 per mm²).

Effects of hANG Gene Transfer on Expression of Other Genes In Vitro and In Vivo Gene Arrays

To assess general effects of hANG gene transfer on tumor cells in vitro and in vivo, the gene expression pattern was studied using gene arrays (Table 1). Because transfer of selection markers such as the hygromycin gene and the selection procedure may cause changes in the genetic program, we analyzed the expression pattern in tumor cell lines as well as in explanted tumors of these cell lines. In general, we found changes in expression of genes related to apoptosis, signal transduction/stress, or metabolism/synthesis (Table 1).

DISCUSSION

Gene transfer of antiangiogenic genes has been suggested as a new strategy of tumor therapy. Benefits of this therapeutic approach are the long-term expression of antiangiogenic genes, which is advantageous for the angio-static character of most antiangiogenic therapies and the genetic stability of endothelium. Another advantage is local production of therapeutic agents at the tumor site, thereby preventing rapid degradation of therapeutic molecules in plasma. Direct effects of hANG overexpression were observed in our coculture experiments with HUVECs, resulting in a decreased proliferation and increased apoptosis rate

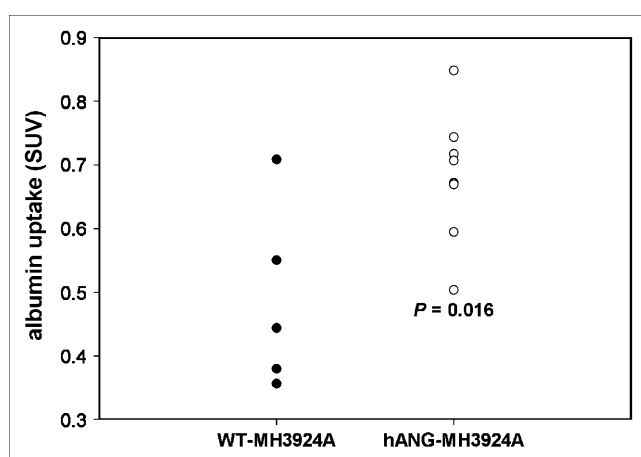


FIGURE 6. ⁶⁸Ga-DOTA-albumin PET: Tumor blood volume of WT-MH3924A ($n = 5$) and hANG-MH3924A ($n = 8$) in ACI rats; 2D acquisition, SUVs were calculated. hANG-overexpressing tumors demonstrated a significant increase in tumor blood volume in comparison with WT-MH3924A.

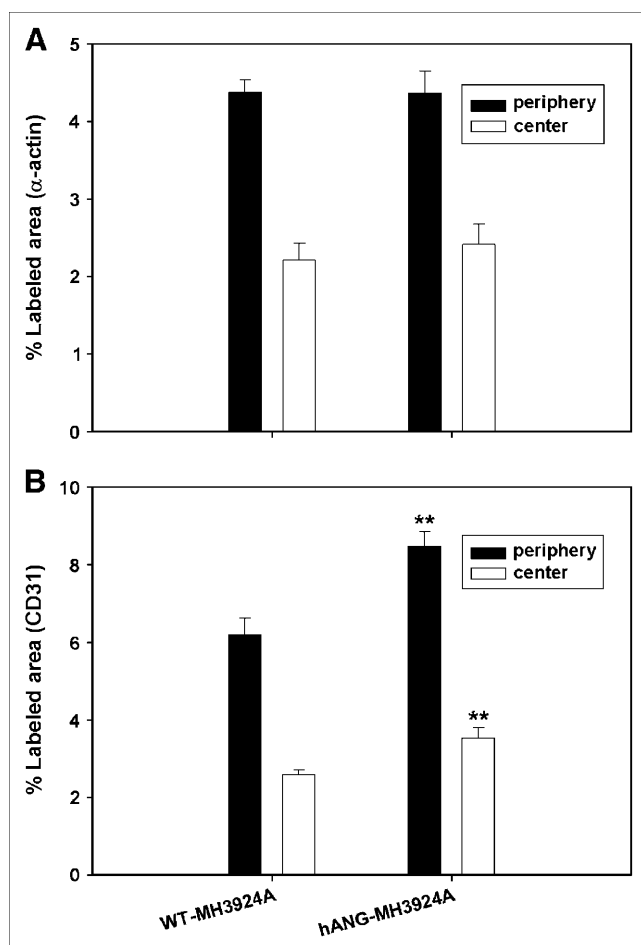


FIGURE 7. Immunohistomorphometric analysis of vascularization in Morris hepatomas. WT-MH3924A and hANG-MH3924A were stained with α -actin or CD31 antibodies (each group, $n = 6$). Control immunoglobulin (data not shown) was used as negative controls. Immunoreactive areas were quantified by analyzing 5 hot spots per tumor. Center = center of tumor. Values are shown as mean \pm SEM (** $P < 0.01$ vs. WT-MH3924A).

of HUVECs compared with coculture with WT-MH3942A cells (Figs. 2A and 2B). Similar results have been demonstrated in HUVECs cocultured with a stable ANG-expressing hepatocellular carcinoma cell line, PLC/PRF/5 (18). Furthermore, these results are in concert with recent reports showing that angiostatin inhibits cell proliferation and induces apoptosis in bovine aortic endothelial cells and HUVECs (19).

We observed a significant inhibition of tumor growth in animals bearing hANG-MH3924A tumors (Fig. 3). Similar results of tumor growth suppression were noted in mice bearing ANG-expressing hepatocellular carcinoma (18) or because of application of recombinant adeno-associated virus encoding ANG plus endostatin using an ovarian cancer cell model (20). Our immunohistochemical analyses indicated decreased proliferation together with an increased apoptosis rate in these tumors (Figs. 4A and 4B), providing additional evidence for antitumoral effects of angiostatin.

The angiogenesis inhibitor is not directly cytotoxic to tumor cells. However, it can increase tumor cell apoptosis and inhibit tumor growth by repressing endothelial cell proliferation/migration or by inducing endothelial cell apoptosis or both (21). Induction of apoptosis may be explained by diminished paracrine release of antiapoptotic factors and increased release of apoptotic factors from endothelial cells into tumor bed.

To assess physiologic changes in tumor perfusion caused by angiostatin, PET studies with $H_2^{15}O$ and ^{68}Ga -DOTA-albumin were performed. $H_2^{15}O$ is perfectly suited for examining tumor tissue perfusion, because it is an inert and freely diffusible molecule not participating in metabolic processes at least during PET measurements (22,23), whereas ^{68}Ga -DOTA-albumin, a tracer of the blood volume, persists in the intravascular space during PET studies. Investigations with $H_2^{15}O$ and ^{68}Ga -DOTA-albumin in hANG-expressing tumors revealed increased tissue perfusion as well as increased blood volumes in comparison with WT-MH3924A (Fig. 5; Fig. 6). The higher tumor-to-heart ratios for $H_2^{15}O$ as compared with albumin are explained by the different distribution of these tracers. The pharmacokinetic model assumes that K_1 is in agreement with blood flow if the extraction rate is high. The model assumes that water is a completely and freely diffusible molecule with 100% extraction from circulation (24). In this model, the fractional DV is the proportion of the ROI in which $H_2^{15}O$ is distributed (25). For example, a value of 2 means that during equilibrium the radioactive concentration in tissue is twice as high compared with that in blood. Because WT- and hANG-expressing tumors did not differ in diameter, changes in tissue perfusion or blood volumes are not due to partial-volume effects. In addition, our PET data are in accordance with our histologic findings that microvessel density is also significantly increased in hANG-overexpressing hepatomas, whereas the fraction of larger vessels (e.g., arterioles) containing α -actin immunoreactive smooth muscle cells was comparable between WT- and hANG-MH3924A tumors (Figs. 7A and 7B). Similar data were obtained with endostatin, where evidence for a dose-dependent biphasic change of tumor perfusion measured by $H_2^{15}O$ PET was found in a phase I clinical trial (26). Lower doses of endostatin resulted in an increase of tumor blood flow, whereas a decrease of tumor blood flow was noted when intermediate or high doses were applied. Improvement of perfusion and dose-dependent response on antiangiogenic agents has been explained by the hypothesis of a decrease in interstitial fluid pressure or normalization of tumor vasculature followed by diminished hypoxia (27). Although it may be speculated that a normalization of tumor vasculature stimulates tumor proliferation, animal and clinical studies to date show no acceleration of tumor growth during antiangiogenic monotherapy despite tumor vessel normalization (27).

We also found that the necrotic area of tumor sections was diminished in hANG-MH3924A. This corresponds to the higher microvessel density and the improvement of

TABLE 1
Changes in Gene Expression in Genetically Modified hANG-Expressing Hepatomas

Gene	Tumor ratio	Cell ratio
Matrix associated		
Tenascin-X	2.66	0.31
Apoptosis associated		
c-myc, exon-2	5.41	1.22
Cyclin-dependent kinase 2- β	4.36	1.33
Rab3 GDP/GTP exchange protein	3.03	4.58
A2b-adenosine receptor	2.63	0.84
Cyclin D3	2.29	0.93
Retinoic acid receptor α 1	2.04	0.82
fos-related antigen (Fra-1)	0.23	0.87
Signal transduction and stress		
γ -Glutamyltranspeptidase	9.96	0.79
Ras-related mRNA rab4	8.51	0.63
α -B-crystallin	5.80	0.36
Angiotensin receptor (AT1)	4.89	0.92
β -1 subunit of Na,K-adenosine triphosphatase	4.08	0.94
Syntaxin 2	3.94	0.94
Cysteine dioxygenase (CDO)	3.64	1.09
SH3-containing protein p4015	3.28	0.41
Phosphatidylinositol 4-kinase	2.97	0.93
Rhodanese	2.96	0.66
Glutathione reductase	2.86	1.57
CLC-7 chloride channel protein	2.75	0.53
Protein kinase C type I	2.74	1.20
Macrophage-stimulating protein	2.71	0.78
Rolipram-insensitive phosphodiesterase type 7 (RPDE7-1)	2.49	0.20
β -B3-2-crystallin	2.47	0.72
Thromboxane A2 receptor	2.26	1.09
Cystathionine γ -lyase (CSE)	2.19	0.87
Adenylyl cyclase type V	2.03	0.97
Macrophage inflammatory protein-1 α	0.39	0.31
Interleukin-1 α	0.38	0.42
Inducible nitric oxide synthase (NOS)	0.33	0.47
Cytochrome P450 IIA2	0.30	1.07
Insulin-like growth factor I	0.30	0.69
Metabolism/synthesis		
UDP glucuronosyltransferase	5.07	1.31
P2X	4.50	0.85
Hepatic microsomal UDP-glucuronosyltransferase (UDPGT)	3.37	1.08
WAP 4-disulfide core domain protein (ps20)	3.27	0.46
Phosphorylase (B-GP1)	2.68	1.25
Bilirubin-specific UDP-glucuronosyltransferase pyruvate dehydrogenase	2.58	0.74
Phosphatase isoenzyme 1	0.34	0.58
Miscellaneous		
α -Actinin-2-associated LIM protein	7.72	0.28
Class Ib RT1	7.25	0.41
MHC class II H- β	6.74	1.26
Factor X	5.56	0.19
Polyprotein 1-microglobulin/bikunin	4.23	0.52
α -1A-adrenergic receptor	3.94	1.94
Memory-related gene-7	3.76	2.41
Nonselective-type endothelin receptor	3.50	0.34
Cell adhesion regulator (CAR1)	3.10	1.11
ϵ 1 globin hereditary hemochromatosis protein	3.06	0.93
Homolog (RT1-CAFe)	2.96	0.98
CD5	2.89	0.74
Melanocyte-specific gene 1 protein (msg1)	2.47	0.82
Chromosomal protein HMG2	2.46	0.40

Ratios of modified vs. WT tumors and cells are shown.

perfusion in these tumors. Therefore, our results imply a better exchange of oxygen and nutrients as well as an improved removal of toxic metabolites from tumor tissue in hANG-overexpressing tumors followed by a decrease of hypoxia but without enhancing tumor growth. Changes in hypoxia may have multiple consequences for the tumor biology, such as promotion of genomic instability (28) and decreased secretion of tumor growth factors. The consequences of hypoxia probably depend on the tumor gene expression level and microenvironment. Additionally, survival of certain tumors cells is based on the same angiogenic growth factors as endothelial cells. This implies that reduction of growth factor levels results in inhibition of tumor and endothelial cell growth inducing tumor regression (27).

With regard to increased vascularization and perfusion in tumors coexisting with significant growth inhibition, vascularization in transfected tumors may not be the limiting factor responsible for tumor growth inhibition. In this context, little attention has been paid to the permeability of blood vessels in tumors. Although the leakiness of tumor vessels is well documented in human cancer and in experimental tumor models, the mechanism is poorly understood (29). It has been shown recently that treatment with ANG for 5 d reduced permeability of tumor blood vessels (30). A reduction of vessel permeability associated with increased microvessel density in hANG-MH3924A tumors may result in an improved functional flow and decreased interstitial fluid pressure preventing hypoxia, a main stimulus of angiogenesis.

The permeability of vessels may be increased by inflammatory mediators and leakage may be related to the migration of leukocytes through vessel walls into tissue (29), producing multiple factors for angiogenesis or inflammation (31). Recently, it was shown that infiltrating CD11(+) cells were the major source of oxidative stress and their cellular infiltration into the tissue corresponded to an enhanced tumor growth (32). Given that the percentage of CD11b(+) cells was significantly diminished in hANG-MH3924A tumors, this finding is compatible with a reduced permeability of the vessels and is interpreted as a decrease of oxidative stress, resulting in diminished growth stimulation.

To assess general escape phenomena of the cells or tumors by changes in the expression pattern, gene array analyses were performed. Gene arrays of the genetically modified cells reveal that overexpression of hANG affects expression of multiple genes. The different gene expression in hANG tumors as compared with hANG cells indicates differences between the *in vitro* situation as opposed to the *in vivo* situation, where the microenvironment—that is, a mixture of cells (hepatoma cells, cells of the vessel wall or of the connective tissue), metabolic interaction of cells, oxygen supply, and so forth—includes potential additional factors. In genetically modified tumors, we found significant changes in a variety of genes related to apoptosis, signal transduction/stress, and metabolism/synthesis.

Tenascin-X regulates the development of blood vessels during vasculogenesis and angiogenesis (33). The observed upregulation of tenascin-X gene expression may be one of the causes for the increase in vascularization or perfusion found in hANG-MH3924A tumors.

The increase in the percentage of apoptotic cells in hANG-MH3924A tumors may be attributed to an induction of several proapoptotic genes in these tumors, such as cyclin-dependent kinase 2 (cdk2) and c-myc, which together have been shown to be critical in the decision between quiescence and apoptosis pathways, sharing regulatory machinery with cell cycle control mechanisms (34). Also, the A2b-adenosine receptor (P1 receptor for adenosine) is involved in apoptosis induction in different cell types (35). Adenosine receptors bind adenosine, which is an ubiquitous nucleoside present in all body cells being released from metabolically active or stressed cells (36).

Modulation of stress-relevant parameters in hANG-MH3924A tumors is evidenced by the increased expression of stress-related genes, such as genes of the cysteine/glutathione-associated or sulfur-delivery metabolism (γ -glutamyltranspeptidase, crystalline, cysteine dioxygenase [CDO], rhodanese, glutathione reductase, cystathionine γ -lyase [CSE]). The increased expression of CSE, CDO (a critical regulator of cysteine concentration), γ -glutamyltranspeptidase (which limits glutathione synthesis by preventing cysteine generation from extracellular glutathione), and glutathione reductase indicates a modulation of the thiol/cysteine/glutathione metabolism by hANG, with a possible impact on the redox state of the tumor-associated cells or apoptosis/proliferation. In this context, overexpression of CSE has been shown recently to inhibit cell proliferation and cell growth (37). Furthermore, rhodanese is believed to function as a sulfur-delivery protein (38) being involved in detoxification of intramitochondrial oxygen free radicals (39). Additionally, we found other stress/signal transduction genes to be elevated in hANG-MH3924A tumors, such as the angiotensin II type 1 (AT1) receptor, which is upregulated in cancer through systemic oxidative stress and hypoxia mechanisms (40).

Finally, we found induction of the expression of several genes coding for enzymes involved in metabolism/synthesis of cholesterol/fatty acids/triglycerides, possibly indicating a high energy expenditure or cell transformation.

CONCLUSION

Transfer of the hANG gene results in inhibition of tumor growth, which may be due to multiple factors such as decreased proliferation, increased apoptosis, and general changes in gene expression. At the genetic level, we observed that hANG induces changes in the expression of multiple genes related mainly to apoptosis, signal transduction or stress, and metabolism. Because these changes in gene expression pattern are predominantly observed in tumor tissue and not *in vitro*, they represent reactions of the

tumor to its changing microenvironment. Furthermore, an increase in perfusion and blood volume was measured in PET studies with H_2^{15}O and ^{68}Ga -DOTA-albumin, corresponding to increased microvessel density and a decrease in necrosis. Therefore, PET studies with these 2 tracers seem to be a sensitive noninvasive tool for the characterization of these changes induced by angiostatin *in vivo*.

ACKNOWLEDGMENTS

The authors thank Helmut Eskerski, Karin Leotta, and Uschi Schierbaum for their help in performing the animal experiments as well as Silke Vorwald and Ulrike Traut for technical assistance in histology. Financial support was from the Wilhelm Sander Stiftung (1999.085.1) and the Tumorzentrum Heidelberg/Mannheim, the Bequest of Herbert Dauss, as well as the Foundation for Cancer and Scarlatina Research.

REFERENCES

- Folkman J. Tumor angiogenesis: therapeutic implications. *N Engl J Med*. 1971;285:1182–1186.
- Bergers G, Benjamin LE. Tumorigenesis and the angiogenic switch. *Nat Rev Cancer*. 2003;3:401–410.
- Kerbel RS. Inhibition of tumor angiogenesis as a strategy to circumvent acquired resistance to anti-cancer therapeutic agents. *Bioessays*. 1991;13:31–36.
- O'Reilly MS, Holmgren L, Shing Y, et al. Angiostatin: a novel angiogenesis inhibitor that mediates the suppression of metastases by a Lewis lung carcinoma. *Cell*. 1994;79:315–328.
- Ji WR, Castellino FJ, Chang Y, et al. Characterization of kringle domains of angiostatin as antagonists of endothelial cell migration, an important process in angiogenesis. *FASEB J*. 1998;12:1731–1738.
- te Velde EA, Vogten JM, Gebbink MF, van Gorp JM, Voest EE, Borel Rinkes IH. Enhanced antitumor efficacy by combining conventional chemotherapy with angiostatin or endostatin in a liver metastasis model. *Br J Surg*. 2002;89:1302–1309.
- Soff GA. Angiostatin and angiostatin-related proteins. *Cancer Metastasis Rev*. 2000;19:97–107.
- Dong Z, Kumar R, Yang X, Fidler IJ. Macrophage-derived metalloelastase is responsible for the generation of angiostatin in Lewis lung carcinoma. *Cell*. 1997;88:801–810.
- McDonald DM, Choyke PL. Imaging of angiogenesis: from microscope to clinic. *Nat Med*. 2003;9:713–725.
- Hoffend J, Mier W, Schuhmacher J, et al. Gallium-68-DOTA-albumin as a PET blood-pool marker: experimental evaluation *in vivo*. *Nucl Med Biol*. 2005;32:287–292.
- Jaffe EA, Nachman RL, Becker CG, Minick CR. Culture of human endothelial cells derived from umbilical veins. identification by morphologic and immunologic criteria. *J Clin Invest*. 1973;52:2745–2756.
- Haberkorn U, Bellemann ME, Brix G, et al. Apoptosis and changes in glucose transport early after treatment of Morris hepatoma with gemcitabine. *Eur J Nucl Med*. 2001;28:418–425.
- Dimitrakopoulou-Strauss A, Strauss LG, Burger C. Quantitative PET studies in pretreated melanoma patients: a comparison of 6- ^{18}F fluoro-L-dopa with ^{18}F -FDG and ^{15}O -water using compartment and noncompartment analysis. *J Nucl Med*. 2001;42:248–256.
- Ohtake T, Kosaka N, Watanabe T, et al. Noninvasive method to obtain input function for measuring tissue glucose utilization of thoracic and abdominal organs. *J Nucl Med*. 1991;32:1432–1438.
- Sharp PE, LaRegina MC. *The Laboratory Rat*. Boca Raton, FL: CRC Press; 1998.
- Schmidt K, Hoffend J, Altmann A, et al. Transfer of the sFLT-1 gene in Morris hepatoma results in decreased growth and perfusion and induction of genes associated with stress response. *Clin Cancer Res*. 2005;11:2132–2140.
- Fox SB, Harris AL. Diagnostic and prognostic significance of tumor angiogenesis. In: Fan TPD, Kohn E, eds. *The New Angiotherapy*. Totowa, NJ: Humana Press Inc.; 2002:151–176.
- Ishikawa H, Nakao K, Matsumoto K, et al. Antiangiogenic gene therapy for hepatocellular carcinoma using angiostatin gene. *Hepatology*. 2003;37:696–704.
- Hanford HA, Wong CA, Kassar H, et al. Angiostatin(4.5)-mediated apoptosis of vascular endothelial cells. *Cancer Res*. 2003;63:4275–4280.
- Isayeva T, Ren C, Ponnazhagan S. Recombinant adeno-associated virus 2-mediated antiangiogenic prevention in a mouse model of intraperitoneal ovarian cancer. *Clin Cancer Res*. 2005;11:1342–1347.
- Folkman J. Angiogenesis and apoptosis. *Semin Cancer Biol*. 2003;13:159–167.
- Bacharach SL, Libutti SK, Carrasquillo JA. Measuring tumor blood flow with H_2^{15}O : practical considerations. *Nucl Med Biol*. 2000;27:671–676.
- Bruehlmeier M, Roelcke U, Schubiger PA, Ametamey SM. Assessment of hypoxia and perfusion in human brain tumors using PET with ^{18}F -fluoromisonidazole and ^{15}O - H_2O . *J Nucl Med*. 2004;45:1851–1859.
- Anderson H, Price P. Clinical measurement of blood flow in tumours using positron emission tomography: a review. *Nucl Med Commun*. 2002;23:131–138.
- Anderson H, Yap JT, Wells P, et al. Measurement of renal tumour and normal tissue perfusion using positron emission tomography in a phase II clinical trial of razoxane. *Br J Cancer*. 2003;89:262–267.
- Herbst RS, Mullani NA, Davis DW, et al. Development of biologic markers of response and assessment of antiangiogenic activity in a clinical trial of human recombinant endostatin. *J Clin Oncol*. 2002;20:3804–3814.
- Jain RK. Normalization of tumor vasculature: an emerging concept in antiangiogenic therapy. *Science*. 2005;307:58–62.
- Nelson DA, Tan TT, Rabson AB, Anderson D, Degenhardt K, White E. Hypoxia and defective apoptosis drive genomic instability and tumorigenesis. *Genes Dev*. 2004;18:2095–2107.
- McDonald DM, Baluk P. Significance of blood vessel leakiness in cancer. *Cancer Res*. 2002;62:5381–5385.
- Satchi-Fainaro R, Mamluk R, Wang L, et al. Inhibition of vessel permeability by TNP-470 and its polymer conjugate, caplostatin. *Cancer Cell*. 2005;7:251–261.
- Carmeliet P. Angiogenesis in health and disease. *Nat Med*. 2003;9:653–660.
- Sluyter R, Halliday GM. Enhanced tumor growth in UV-irradiated skin is associated with an influx of inflammatory cells into the epidermis. *Carcinogenesis*. 2000;21:1801–1807.
- Ikuta T, Ariga H, Matsumoto K. Extracellular matrix tenascin-X in combination with vascular endothelial growth factor B enhances endothelial cell proliferation. *Genes Cells*. 2000;5:913–927.
- Helbing CC, Wellington CL, Gogela-Spehar M, Cheng T, Pinchbeck GG, Johnston RN. Quiescence versus apoptosis: Myc abundance determines pathway of exit from the cell cycle. *Oncogene*. 1998;17:1491–1501.
- Le Poole IC, Yang F, Brown TL, et al. Altered gene expression in melanocytes exposed to 4-tertiary butyl phenol (4-TBP): upregulation of the A2b adenosine receptor 1. *J Invest Dermatol*. 1999;113:725–731.
- Ohana G, Bar-Yehuda S, Barer F, Fishman P. Differential effect of adenosine on tumor and normal cell growth: focus on the A3 adenosine receptor. *J Cell Physiol*. 2001;186:19–23.
- Yang G, Cao K, Wu L, Wang R. Cystathionine gamma-lyase overexpression inhibits cell proliferation via a H₂S-dependent modulation of ERK1/2 phosphorylation and p21Cip/WAK-1. *J Biol Chem*. 2004;279:49199–49205.
- Ogasawara Y, Lacourciere G, Stadtman TC. Formation of a selenium-substituted rhodanese by reaction with selenite and glutathione: possible role of a protein perselenide in a selenium delivery system. *Proc Natl Acad Sci U S A*. 2001;98:9494–9498.
- Nandi DL, Horowitz PM, Westley J. Rhodanese as a thioredoxin oxidase. *Int J Biochem Cell Biol*. 2000;32:465–473.
- Smith GR, Missailidis S. Cancer, inflammation and the AT1 and AT2 receptors. *J Inflamm (Lond)*. 2004;1:3–15.



The Journal of
NUCLEAR MEDICINE

Angiostatin Overexpression in Morris Hepatoma Results in Decreased Tumor Growth but Increased Perfusion and Vascularization

Kerstin Schmidt, Johannes Hoffend, Annette Altmann, Ludwig G. Strauss, Antonia Dimitrakopoulou-Strauss, Britta Engelhardt, Dirk Koczan, Jörg Peter, Thomas J. Dengler, Walter Mier, Michael Eisenhut, Uwe Haberkorn and Ralf Kinscherf

J Nucl Med. 2006;47:543-551.


This article and updated information are available at:
<http://jnm.snmjournals.org/content/47/3/543>

Information about reproducing figures, tables, or other portions of this article can be found online at:
<http://jnm.snmjournals.org/site/misc/permission.xhtml>

Information about subscriptions to JNM can be found at:
<http://jnm.snmjournals.org/site/subscriptions/online.xhtml>

The Journal of Nuclear Medicine is published monthly.
SNMMI | Society of Nuclear Medicine and Molecular Imaging
1850 Samuel Morse Drive, Reston, VA 20190.
(Print ISSN: 0161-5505, Online ISSN: 2159-662X)

© Copyright 2006 SNMMI; all rights reserved.

 SOCIETY OF
NUCLEAR MEDICINE
AND MOLECULAR IMAGING